

# Optical Engineering

[SPIDigitalLibrary.org/oe](http://SPIDigitalLibrary.org/oe)

## **Experimental observation of spatial correlation of scintillations from an extended incoherent source**

Ingmar G. E. Renhorn  
Thomas Svensson  
Glenn D. Boreman

# Experimental observation of spatial correlation of scintillations from an extended incoherent source

**Ingmar G. E. Renhorn**  
**Thomas Svensson**

FOI—Swedish Defense Research Agency  
P.O. Box 1165, SE-581 11  
Linköping, Sweden  
E-mail: [ingmar.renhorn@foi.se](mailto:ingmar.renhorn@foi.se)

**Glenn D. Boreman**

University of North Carolina at Charlotte  
Department of Physics and Optical Science  
Charlotte, North Carolina 28223

**Abstract.** The optical irradiance scintillation for an extended source and a dual-aperture system with variable aperture separation is analyzed with respect to the effect of turbulence. The scintillation index and the correlation between the dual-aperture signals emanating from an extended source are used to study the turbulence spectral model and the deviation from the common Kolmogorov atmospheric weak-turbulence model. Signal decorrelation as a function of aperture separation is presented. The relative errors introduced by using dual-aperture systems are also discussed. © The Authors. Published by SPIE under a Creative Commons Attribution 3.0 Unported License. Distribution or reproduction of this work in whole or in part requires full attribution of the original publication, including its DOI. [DOI: [10.1117/1.OE.52.2.026001](https://doi.org/10.1117/1.OE.52.2.026001)]

Subject terms: atmospheric turbulence; imaging through turbulent media; infrared imaging.

Paper 121627 received Nov. 7, 2012; revised manuscript received Dec. 20, 2012; accepted for publication Dec. 21, 2012; published online Feb. 4, 2013.

## 1 Introduction

Measurements of source radiation through turbulent atmosphere are needed in many applications. Applications range from free-space communication using laser beams to remote sensing and astronomy.<sup>1–3</sup> The accuracy of these measurements is influenced by both spatial and temporal fluctuations, making radiometric measurements difficult. In free-space communication, signal fading is partially mitigated by using large-aperture averaging or by combining several apertures at separations where the irradiance is considered uncorrelated. In practice, it is often not possible to obtain fully uncorrelated signals. In other applications, such as simultaneous measurements in different spectral bands, fully correlated signals are desired.<sup>4</sup> Here, the intended primary application is a dual-color, dual-polarimetric, or other dual-parametric wide field of view imaging system. In these applications, dual apertures with small diameters will result in increased uncertainty due to signal decorrelation between the two channels. Even when the two apertures are close to each other, substantial decorrelation can occur. The realization of systems using dual apertures is sometimes more practical than dual-channel, single-aperture systems. The dual-color focal plane technology is less mature, with substantial cross-talk between the spectral channels, and the sensor arrays have fewer pixels than corresponding single-color systems. In remote sensing applications, spatial resolution is of primary value, so large focal plane arrays are required. For this reason, it is important to study the impact of decorrelation of intensity fluctuations on the performance of dual-aperture systems in comparison to the dual-color, single-aperture systems. Useful parameters in this context are the decorrelation length of intensity fluctuations and the decorrelation time of intensity fluctuations. However, the decorrelation time is strongly dependent on wind speed and platform motion. Signal decorrelation will be influenced by the aperture size and separation, integration time, range to the source, and source size. It will also depend strongly on the geometrical arrangement of the transmitter and receiver, whether it is a ground-to-ground, ground-to-air, or air-to-ground scenario.

The optical irradiance scintillation for an extended source and extended receiver has been studied previously, and observations have been compared to a physics-based model.<sup>5</sup> The source and receiver are considered extended with respect to the corresponding Fresnel zone size. The optical irradiance scintillation in a dual-aperture system with variable aperture separation can be used to analyze the effect of turbulence. The irradiance scintillation index and the correlation between the dual-aperture signals can be used to study the turbulence spectral model and the potential deviation from the common Kolmogorov atmospheric weak-turbulence model.<sup>6</sup> In this study, we use a large source that filters the high spatial frequencies and places the measurement situation in the weak-turbulence domain.<sup>7</sup> We assume that the turbulence is locally stationary.<sup>8</sup> The fundamental parameters obtained from the experiments are  $C_n^2$ , the generalized refractive-index structure constant, and the spectral power-law parameter  $\alpha$ , for which a variation around the Kolmogorov value of  $\alpha = 11/3$  is investigated.

The experimental work is described in Sec. 2. The theory for the covariance signal and relative errors for a conceptual dual-channel system are presented in Secs. 3 and 4. The experimental results are given in Sec. 5, and the implications for a dual-channel system in various scenarios are discussed in Sec. 6.

## 2 Experimental Setup

The trial was performed in September 2011. The receiver was located in an elevated window of a building, with the source at a range of 2.5 km. The propagation path was over an inhomogeneous area with buildings nearby and both roads and grass fields in between. Three apertures at different separations were used in order to obtain simultaneous decorrelation measurements at three distances. A meteorological station was placed close to the camera (about 10 m). Weather data were logged every 5 min.

Scintillation data were collected at a frame rate of 200 frames/s with an MWIR camera in the spectral range of 4.6 to 5.1  $\mu\text{m}$  (defined by the combined passband of

the detector and an optical filter). The camera is based on an InSb  $640 \times 512$  pixels array with an NETD ( $300 \text{ K}$ )  $< 20 \text{ mK}$  at an integration time of  $3 \text{ ms}$ . The full frame rate is  $50 \text{ frames/s}$ ; a rate of  $200 \text{ frames/s}$  was reached using subwindowing ( $320 \times 256$  pixels). The pixel size is  $20 \times 20 \mu\text{m}^2$ , and the pixel pitch is  $24 \mu\text{m}$ . For measurement purposes, narrow field of view optics were selected. Using a  $F/2.9$  lens with an effective focal length of  $250 \text{ mm}$  results in a field of view of  $3.5 \times 2.8 \text{ deg}$  and an instant field of view of  $0.096 \text{ mrad}$ . Each collected data file from the camera contained  $1,000$  frames, which corresponds to an acquisition sequence of  $5 \text{ s}$ . A hotplate was used as a source. It had an approximate temperature of  $820^\circ\text{C}$  and a low-emissivity aperture plate made of aluminum to define a source diameter of  $20 \text{ cm}$ .

The hotplate was placed  $1.5 \text{ m}$  above the ground. To get a free line of sight, scintillation data were collected  $12.5 \text{ m}$  above the ground. Two lens covers were made with three apertures ( $\varnothing = 20 \text{ mm}$ ) at different center-to-center separations between the apertures. In two of the apertures,  $\text{CaF}_2$  wedge prisms were mounted; one aperture was left empty. The wedge angles of the prisms were  $20 \text{ mrad}$  and  $40 \text{ mrad}$ . Sketches of the two lens covers are shown in Fig. 1. Recorded frames show three images of the source, where each image is associated with one aperture (Fig. 2). Five sets of scintillation data were collected. Camera settings and collected weather parameters for one data set (representative for the trial) are displayed in Table 1. No interpolation of the weather data, logged at  $5\text{-min}$  intervals, has been performed in the table.

The collected source data were processed by summing the pixels over each image of the hotplate source, typically  $7 \times 7$  pixels, which yielded the digital sum of the target and the local background. The integrated signal due to the target was then obtained by subtracting the local background. The latter was estimated by calculating the average of the pixels surrounding the  $49$  pixels over the hotplate, multiplied by  $49$ . The integration time is short, and the “frozen” atmosphere is assumed to be sampled. For a moving platform, the integration time can be of similar magnitude as the decorrelation time. However, this subject is not treated here. The variations in weather parameters were rather small. The wind, including cross-wind, was measured using the local weather station. The cross-wind could also be estimated using the delayed correlation of the signals from the dual

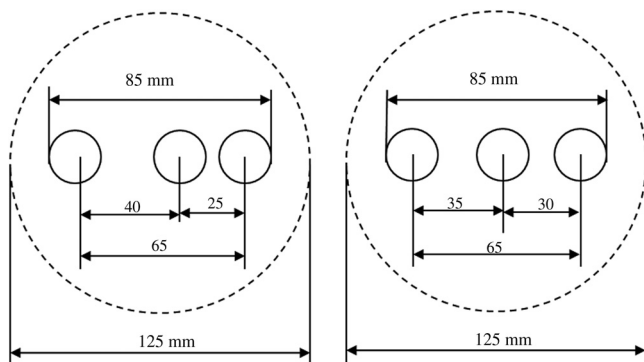


**Fig. 1** Sketches of the two lens covers. Two wedge prisms (wedge angles  $40 \text{ mrad}$  and  $20 \text{ mrad}$ ) were mounted in the left and middle apertures, respectively. The right aperture was left empty. The diameter of each aperture was  $20 \text{ mm}$ .

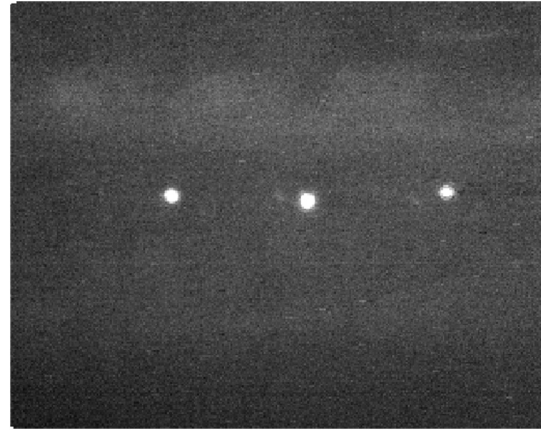


**Fig. 2** One frame collected during the second trial showing three instantaneous images of the hotplate source.

apertures. This is not the main topic here, and we will not elaborate on it further.

### 3 Theory

#### 3.1 Correlation and Covariance

The normalized spatial covariance of the irradiance scintillation is defined by

$$C(\rho) = \frac{\langle [I(r) - \langle I(r) \rangle][I(r + \rho) - \langle I(r + \rho) \rangle] \rangle}{\langle I(r) \rangle \langle I(r + \rho) \rangle}, \quad (1)$$

where  $I(r)$  [ $\text{W m}^{-2}$ ] is the irradiance,  $r$  [m] is the transverse coordinate, and  $C(0)$  is the normalized irradiance variance or the scintillation index. Thus,

$$C(0) = \sigma_I^2 = \frac{\langle I^2 \rangle}{\langle I \rangle^2} - 1. \quad (2)$$

For an extended source and an extended receiver, the covariance is given by Hill and Ochs<sup>9</sup> as

$$C(\rho) = 16\pi^2 k^2 \times \int_0^\infty \int_0^1 \kappa \Phi_n(\kappa) \sin^2 \left[ \frac{\kappa^2 L u (1 - u)}{2k} \right] \times \left\{ \frac{2J_1[\kappa r_t (1 - u)]}{\kappa r_t (1 - u)} \frac{2J_1[\kappa r_r u]}{\kappa r_r u} \right\} J_0(\kappa \rho u) du d\kappa, \quad (3)$$

where  $r_t$  and  $r_r$  are the transmitter radius and receiver radius, respectively, and  $u$  is a dimensionless variable of path distance normalized by the range  $u = z/L$ .

The correlation coefficient is given by

$$\gamma(\rho) = \frac{C(\rho)}{C(0)}. \quad (4)$$

The correlation coefficient, a direct measure of the similarity of the fluctuations of the irradiance at the two apertures at distance  $\rho$ , varies between zero and one.

The weak nonKolmogorov turbulence spectrum is given by Cui et al.<sup>10</sup> as

$$\Phi_n(\kappa, \alpha) = \frac{\Gamma(\alpha - 1)}{4\pi^2} \cos\left(\frac{\alpha\pi}{2}\right) C_n^2 \kappa^{-\alpha}, \quad (5)$$

**Table 1** The second trial.  $\Delta$  = center-to-center separation [mm] between the apertures in the lens cover. The table shows one of the five sets of scintillation data that were collected.

Data set	Aperture separations [mm]	Int. time [ms]	Solar radiation [W/m <sup>2</sup> ]	Temperature [°C]	Wind speed [m/s]	Wind dir. [°]	Cross-wind [m/s]
1	$\Delta = 25, 40, 65$	1.0	531	14.2	3.8	286	1.8
2	$\Delta = 30, 35, 65$	1.0	560	14.0	4.6	279	2.7
3	$\Delta = 25, 40, 65$	2.0	531	14.2	3.8	286	1.8
4	$\Delta = 30, 35, 65$	2.0	560	14.0	4.6	279	2.7
5	$\Delta = 25, 40, 65$	3.0	531	14.2	3.8	286	1.8
6	$\Delta = 30, 35, 65$	3.0	560	14.0	4.6	279	2.7

where the Kolmogorov spectrum is a special case given by  $\alpha = 11/3$ , and the parameter  $\kappa$  is the spatial wavenumber. In the analyses below, the spectral power law parameter  $\alpha$  has been varied around  $11/3$ , fitting the experimentally observed cross-correlation.  $C_n^2$  is the generalized refractive-index structure constant with a value that varies with  $\alpha$  and with units of  $\text{m}^{3-\alpha}$ .

### 3.2 Error Analysis

An important application of the dual-channel measurements is spectral angle measurements. This technique has proven valuable in remote sensing and can be used, for example, to suppress background clutter. The error in spectral angle matching is related to the quotient of  $x$  and  $y$ , which therefore becomes an important parameter of merit. This measurement function is described by  $g(x, y) = x/y$ , where the signal  $x$  emanates from one of the apertures, and  $y$  emanates from a second aperture at a specific distance from the first.

The fractional error is given by Barlow<sup>11</sup> as

$$\frac{\sigma_g^2}{g^2} = \frac{\sigma_x^2}{x^2} + \frac{\sigma_y^2}{y^2} - 2 \frac{\sigma_{xy}}{xy}, \quad (6)$$

where  $\sigma_g^2$ ,  $\sigma_x^2$ , and  $\sigma_y^2$  are the variances and  $\sigma_{xy}$  is the correlation between the signals  $x$  and  $y$ . If the signals are independent, a change in one channel does not imply an expected change in the other. When the correlation coefficient between the two signals is equal to one, the error decreases to

$$\frac{\sigma_g^2}{g^2} = \left( \frac{\sigma_x}{x} - \frac{\sigma_y}{y} \right)^2. \quad (7)$$

When measurements are performed at different wavelengths, a slight increase in decorrelation can occur. Therefore, the estimate using the same wavelength for both apertures can be considered a lower limit to the error. In the analysis here, the decorrelation is assumed to be the primary cause of errors.

## 4 Results

Measurements using three apertures at different separation distances (as shown in Fig. 1) were used to obtain

simultaneous decorrelation measurements at three distances. The level of turbulence was determined from the observed scintillation index knowing the aperture sizes and the propagation distance. All three apertures give the same scintillation index. The correlated signal distribution from the two apertures at a distance of 30 and 65 mm is shown in Fig. 3. The level of turbulence is estimated to  $C_n^2 = 3.110^{-14} \text{ m}^{-2.6/3}$  from the scintillation index using the nonKolmogorov model with  $\alpha = 11.6/3$ , and the range is  $L = 2,460$  m. The method is described by Renhorn et al.<sup>5</sup>

The signal probability distribution is shown in Fig. 4. Because of large-source filtering, the atmospheric turbulence causes weak fluctuations, and simplified models that do not take saturation into account can be used. The scintillation index is in this case is  $\sigma_I^2 = 0.035$ .

The intensity weak-fluctuation spectrum can give indications of the power law behavior. The purpose of introducing the intensity fluctuation spectrum is to motivate the disregarding of the inner scale in the subsequent treatment. It will not be further used after that. Locally isotropic Kolmogorov spectra are considered scaled by  $W(f) \cong f^{-8/3}$  in the inertial subrange,<sup>12</sup> where  $W(f)$  is the normalized intensity fluctuation spectrum of irradiance and  $f$  is the temporal frequency. The intensity spectrum of these measurements is shown in Fig. 5. The dissipation region, which is expected to have a higher slope, is filtered out by the large source size. As a result, the inner scale does not influence the measured statistics.

In Fig. 6, a comparison of observed covariance as a function of aperture distance is made with theory. A nonKolmogorov model has been assumed with a power law exponent  $\alpha$  that varies with the measurement conditions. The only other variable in the comparison between observation and theory is the structure parameter of refractive index fluctuations,  $C_n^2$ . It is therefore interesting to compare normalized covariance at various levels of turbulence as in Fig. 6.

## 5 Discussion

The large source compared to the almost point-sized receiver results in an asymmetric weighting of the influence of turbulence with respect to range. The path-weighting function for the present system is shown in Fig. 7. The most important range is at approximately 20% of the total range to the

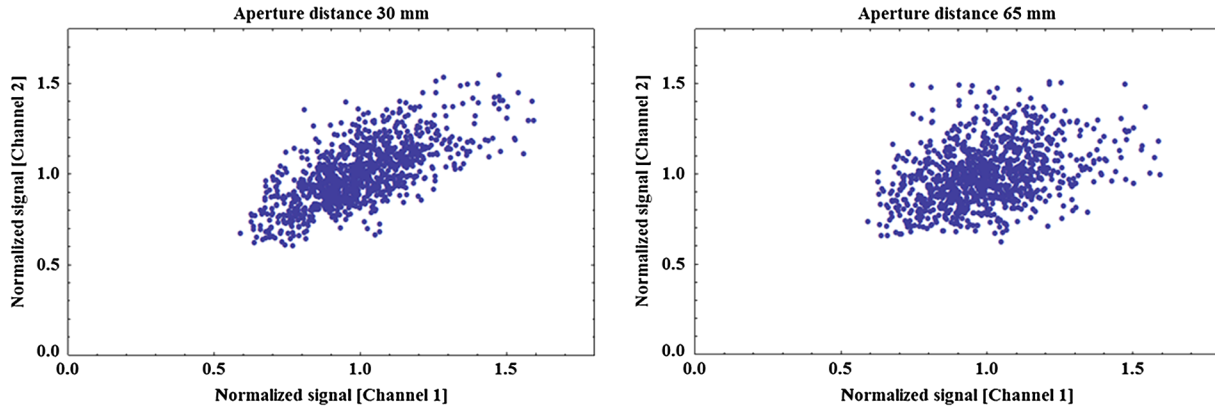


**Fig. 3** Normalized signal distribution at aperture distances of 30 mm and 65 mm. Channel 1 corresponds to the signal from the first aperture, and channel 2 corresponds to the synchronously measured signal from the second aperture. The level of turbulence is  $C_n^2 = 3.110^{-14} \text{ m}^{-2.6/3}$ , and the range is  $L = 2,460 \text{ m}$ . The signal distribution for aperture distances of 25, 35, and 40 mm follow a similar trend as shown here.

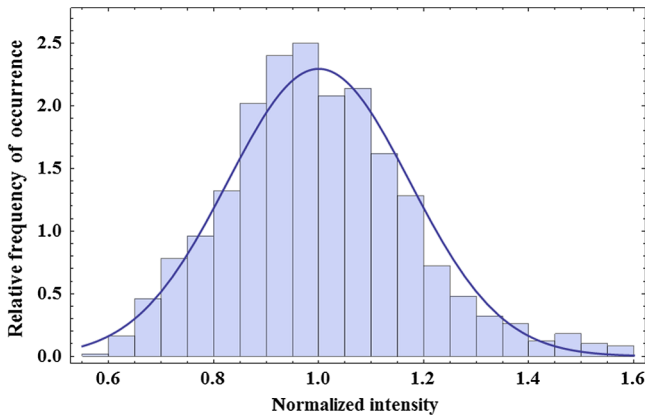


**Fig. 4** Typical normalized signal distribution compared to a normal distribution. The histogram is scaled to a probability density function. The estimated level of turbulence is  $C_n^2 = 3.110^{-14}$  and  $\sigma_f^2 = 0.035$ .

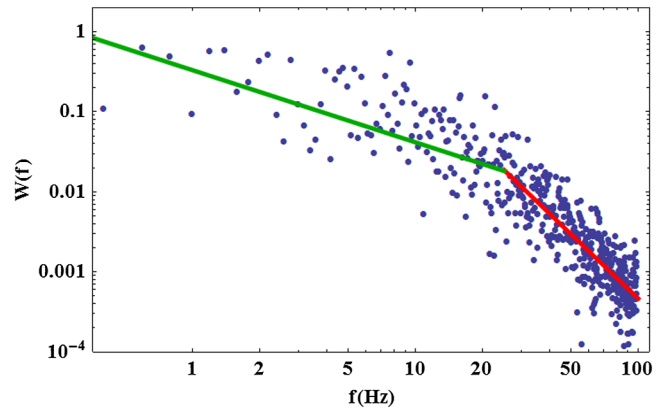


**Fig. 5** Experimental observation of the intensity fluctuation spectrum. The green line corresponds to the low-frequency region, and the red line corresponds to the inertial region with an expected  $8/3$  slope. The observed slope is slightly lower than the expected slope.

source. Thus, the measurement geometry has a strong impact on the observed effect of turbulence. In this case, the measurements have been performed in a ground-to-ground scenario. Applications are anticipated in both ground-to-ground and air-to-ground scenarios. In an air-to-ground scenario, the influence of turbulence will be much smaller, due to the decreasing level of turbulence with altitude. Therefore, it is of interest to estimate the influence of turbulence on the measurement accuracy with respect to an airborne system. The range-dependent path-weighting function of the influence of turbulence is shown in Fig. 7. The weighting function is inherent in the covariance function shown in Eq. (3).

There are many models being used by the optical community for the altitude dependence of the  $C_n^2(h)$  parameter,<sup>13</sup> where  $h$  is the altitude. The level of turbulence is considered relatively constant in the surface layer. The height of the surface layer can vary from meters during stable conditions to hundreds of meters during strongly unstable convective conditions.<sup>14</sup> The altitude dependence of turbulence is modeled (as shown in Fig. 8) by the Hufnagel-Valley model described by Andrews, Phillips, and Yu<sup>15</sup> as

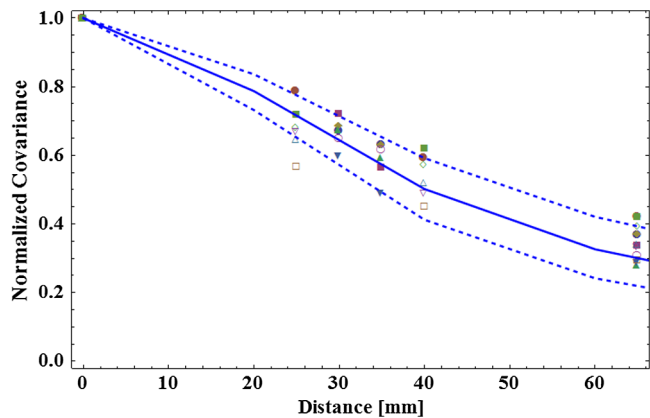


**Fig. 6** Comparison of normalized covariance for a slant path from a building over an inhomogeneous area. The solid line shows the model prediction using a spectral power law parameter  $\alpha = 11/3$ . The upper dashed line is for  $\alpha = 12/3$ , and the lower dashed line is for  $\alpha = 10/3$ . The turbulence levels varied between  $C_n^2 = 0.475 \times 10^{-14}$  and  $2.43 \times 10^{-14}$  with a mean value of  $1.40 \times 10^{-14}$ . The observations indicate that the similarity is high, at least under stable turbulence conditions. The range is  $L = 2,460 \text{ m}$ .

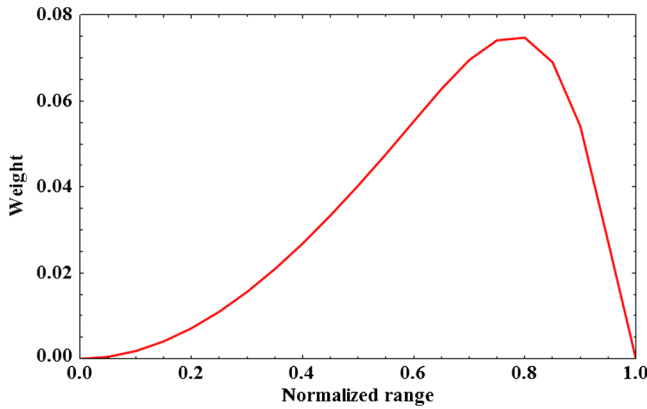


**Fig. 7** Range-dependent path-weighting function of the influence of turbulence using the Kolmogorov spectrum. The source radius is 0.115 m, and the receiver radius is 0.01 m.

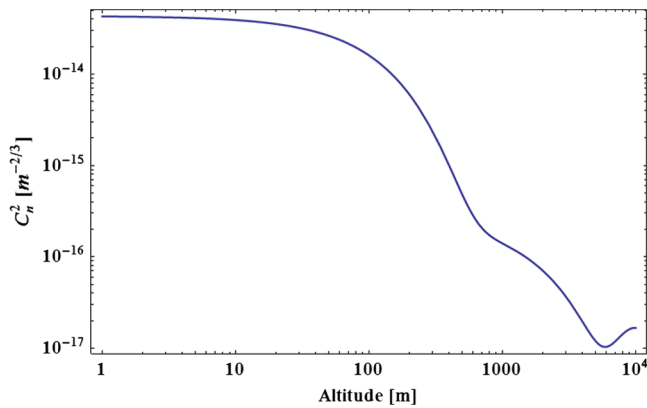


**Fig. 8** Change in turbulence with altitude. Turbulence drops rapidly above 100 m.

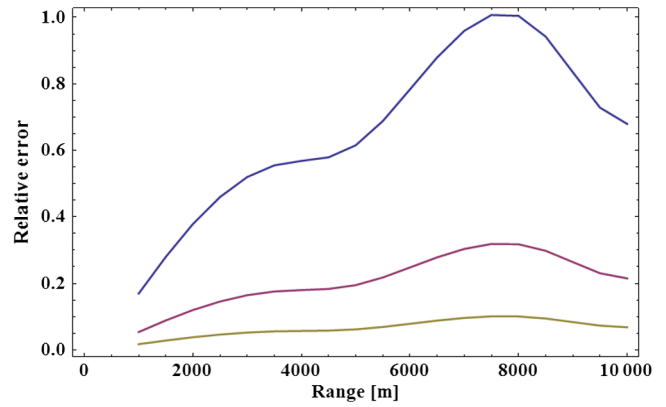
$$C_n^2(h) = 0.00594 \left(\frac{v}{27}\right)^2 (h \times 10^{-5})^{10} \exp\left(-\frac{h}{1000}\right) + 2.7 \times 10^{-16} \exp\left(-\frac{h}{1500}\right) + A \exp\left(-\frac{h}{100}\right), \quad (8)$$

with  $A \approx C_n^2(0) \text{ m}^{-2/3}$  and  $v = 21 \text{ m/s}$ .

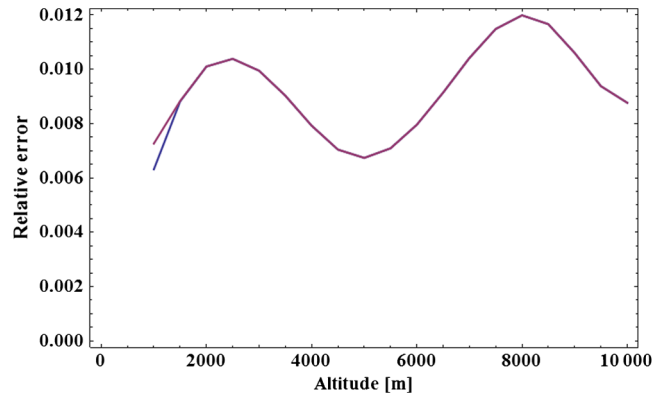
The relative error using equally sized apertures is given by  $\sqrt{\sigma_f^2/f^2} = \sqrt{2[C(0) - C(\rho)]}$ , where  $C(\rho)$  is obtained from Eq. (3). The relative error has been calculated for an aperture separation of 25 mm and an aperture diameter of 20 mm at three different levels of turbulence. For the ground-to-ground application, the influence of turbulence is already substantial at quite low levels of turbulence. This is exemplified by  $C_n^2 = 10^{-14} \text{ m}^{-2/3}$  as illustrated in Fig. 9.

Figure 10 exemplifies the improvement in accuracy of an airborne system compared with a ground-based system. Even when the turbulence at ground level is high, the influence on system performance is rather limited.

In Figs. 9 and 10, the strong dependence of the level of turbulence on the error is exemplified. In the ground-to-ground scenario, the error increases even at rather low levels of turbulence, making a dual-aperture classification system based on two spectral bands sensitive to errors. A single-aperture system will be able to suppress turbulence-induced



**Fig. 9** Relative error (1 std) for a dual-aperture system with a diameter of 0.01 m separated by 0.025 m at turbulence levels of  $C_n^2 = 10 \times 10^{-14} \text{ m}^{-2/3}$  (upper curve),  $1 \times 10^{-14} \text{ m}^{-2/3}$  (middle curve), and  $0.1 \times 10^{-14} \text{ m}^{-2/3}$  (lower curve) as a function of range.



**Fig. 10** Relative error (1 std) for a dual-aperture system with a diameter of 0.01 m separated by 0.025 m at a turbulence level of  $C_n^2 = 100$  and  $1 \times 10^{-14} \text{ m}^{-2/3}$  as a function of altitude. For altitudes above 1,500 m, the relative error is independent of ground level turbulence, and the two curves are superimposed on each other. For low altitudes, a higher level of turbulence will result in a higher relative error.

errors to a much higher degree but at a cost of a much more complex sensor system and often a lower number of imaging pixels. For an airborne system, the level of turbulence is generally much lower, and even though the covariance as a function of aperture distance is basically the same as it is for the ground-based sensor, the influence of turbulence is much lower. A dual-aperture system is therefore viable in these applications.

## 6 Conclusions

The cross-correlation of optical signals in weak turbulence has been studied assuming locally wide-sense stationarity over the 5-s measurement intervals. Due to the large source, the dissipation region of the turbulence spectrum is not sampled. The detrimental effect of turbulence on dual-aperture and dual-color instrumentations for ground-to-ground applications is observed. In the present tests with a spatially extended source, the turbulence at a range of approximately 20% of the total range from the sensor to the target is emphasized, as can be observed from the path-weighting function shown in Fig. 7. This results in an expected decrease in relative error with sensor altitude, as shown in Figs. 9 and 10.

Dual-aperture systems are therefore an alternative for airborne systems, but similar systems will suffer strong degradation when used in ground-to-ground applications. A trend toward single-aperture systems can be expected, initially for low-altitude applications. Dual-color focal plane arrays still suffer from reduced fill-factor and/or cross-talk between spectral channels in the MWIR spectral region. The number of pixels also has to increase compared with single-color focal plane arrays. With increased spatial resolution comes the possibility to suppress false classifications from the size of the source.

The results here can serve as one component in a trade-off study concerning classification based on size, spectral properties, and temporal properties.

## References

1. L. C. Andrews and R. L. Phillips, *Laser Beam Propagation through Random Media*, SPIE Press, Bellingham, WA (1998).
2. N. S. Kopeika, *A System Engineering Approach to Imaging*, SPIE Press, Bellingham, WA (1998).
3. M. C. Roggemann and B. Welsh, *Imaging Through Turbulence*, CRC Press Inc., Boca Raton, Florida (1996).
4. J. H. Churnside, R. J. Lataitis, and J. J. Wilson, "Two-color correlation of atmospheric scintillation," *Appl. Opt.* **31**(21), 4285–4290 (1992).
5. I. G. E. Renhorn et al., "Infrared image scintillation: comparison of modeling and measurement," *Opt. Eng.* **45**(1), 016001 (2006).
6. R. G. Frehlich, "Estimation of the parameters of the atmospheric turbulence spectrum using measurements of the spatial intensity covariance," *Appl. Opt.* **27**(11), 2194–2198 (1988).
7. E. L. Bass, B. D. Lackovic, and L. C. Andrews, "Aperture averaging of optical scintillations based on a spectrum with high wave number bump," *Opt. Eng.* **34**(1), 26–31 (1995).
8. V. I. Tatarskii, *Wave Propagation in a Turbulent Atmosphere*, McGraw-Hill, New York (1961).
9. R. J. Hill and G. R. Ochs, "Fine calibration of large-aperture optical scintillometers and an optical estimate of inner scale of turbulence," *Appl. Opt.* **17**(22), 3608–3612 (1978).
10. L. Cui et al., "Atmospheric spectral model and theoretical expressions of irradiance scintillation index for optical wave propagation through moderate-to-strong non-Kolmogorov turbulence," *J. Opt. Soc. Am. A* **29**(6), 1091–1098 (2012).
11. R. J. Barlow, *Statistics*, John Wiley & Sons Ltd., West Sussex, England (1989).
12. R. Rao et al., "Turbulence spectrum effect on wave temporal-frequency spectra for light propagating through the atmosphere," *J. Opt. Soc. Am. A* **16**(11), 2755–2762 (1999).
13. R. R. Beland, "Propagation through atmospheric turbulence," Chapter 2 in *The Infrared and Electro-Optical Systems Handbook*, F. G. Smith, ed., SPIE Optical Engineering Press, Bellingham, WA, Vol. 2 (1993).
14. D. L. Hutt, "Modeling and measurements of atmospheric optical turbulence over land," *Opt. Eng.* **38**(8), 1288–1295 (1999).
15. L. C. Andrews, R. L. Phillips, and P. T. Yu, "Optical scintillation and fade statistics for a satellite-communication system," *Appl. Opt.* **34**(33), 7742–7751 (1995).



**Ingmar G. E. Renhorn** is research director for IR and EO systems at the Swedish Defense Research Agency (FOI) at Linköping, Sweden, where he has been a staff scientist since 1981. In 1994, he was appointed director of research in the Department of IR Systems. His fields of major interest include multi/hyperspectral imaging systems, thermal imaging, atmospheric effects on imaging systems (including turbulence and aerosol profiling), imaging theory, image and signal processing, optical information processing, signature measurement, and sensor systems with applications in reconnaissance, infrared search and track, target acquisition, and optical warning. He is a member of SPIE.



**Thomas Svensson** received his MSc in chemical engineering at the Lund Institute of Technology, where he received his PhD in 2001. His main research focus was on FTIR spectroscopic studies of molecular complexes of atmospheric interest. He joined the Swedish Defence Research Agency (FOI) in 2001 and has been working since then with multi/hyperspectral imaging systems, image processing, and measurements of electro-optical signatures, in particular thermal infrared signatures. His current research interests include characterization and applications of electro-optical imaging systems. He is a member of SPIE.



**Glenn D. Boreman** is the chairman of the Department of Physics and Optical Science at University of North Carolina at Charlotte. He received a BS from Institute of Optics, University of Rochester, and a PhD from the Optical Sciences Center, University of Arizona. From 1984 to 2011, he served on the faculty of University of Central Florida, where he held the Trustee Chair Professorship in Optics for eight years. He has supervised 33 MS and 24 PhD students to completion. He has published more than 150 journal articles and three textbooks (*Infrared Detectors and Systems*, *Basic Electro-Optics for Engineers*, and *Modulation Transfer Function in Electro-Optical Systems*). He has been a visiting scholar at Imperial College (London), ETH (Zürich), the Swedish Defense Research Agency (Linköping, Sweden), and Universidad Complutense (Madrid). He is a Fellow of the Optical Society of America, SPIE, and the Military Sensing Symposium.